NOTE

Locating cryptotephra in lake sediments using fluid imaging technology

Robert M. D'Anjou · Nicholas L. Balascio · Raymond S. Bradley

Abstract We report a new approach to locate and quantify cryptotephra in sedimentary archives using a continuously-imaging Flow Cytometer and Microscope (FlowCAM®). The FlowCAM rapidly photographs particles flowing in suspension past a microscope lens and performs semi-automated analysis of particle images. It has had primarily biological applications, although the potential sedimentological applications are numerous. Here we test the ability of this instrument to image irregularly shaped, vesicular glass shards and to screen sediment samples for the presence of cryptotephra. First, reference samples of basalt and rhyolite tephra (sieved <63 μm) were analyzed with the FlowCAM, demonstrating the ability of the instrument to photograph individual tephra shards. The highest-quality images were used to create a reference library of tephra particles, against which other particle morphologies could be automatically compared. Lake sediment samples with known concentrations of tephra were then analyzed. The tephra image library was used to perform pattern recognition calculations, automatically distinguishing tephra-like images from other particles in the sediment samples. The number of tephra shards identified by the FlowCAM technique was compared to manual counting using a polarizing light microscope, demonstrating that this rapid approach is capable of determining the relative concentrations of tephra in a given sediment sample. However, the FlowCAM systematically underestimates tephra concentrations relative to manual counts. We conclude that with a well-developed image library, the FlowCAM can be an effective tool for cryptotephra and sedimentological applications, but it may be inappropriate for large volume samples or if particle morphologies are outside the range of the image library.

Keywords Tephra · Cryptotephra · Lake sediment · Fluid imaging · Particle recognition · FlowCAM

R. M. D'Anjou · N. L. Balascio (✉) · R. S. Bradley
Department of Geosciences, Climate Systems Research Center, University of Massachusetts Amherst, Amherst, MA 01003, USA
e-mail: balascio@ldeo.columbia.edu

Present Address:
N. L. Balascio
Lamont-Doherty Earth Observatory of Columbia University, Palisades, NY 10964, USA

Introduction

Tephrochronology plays a valuable role in paleoenvironmental studies by providing time markers in the form of volcanic ash (tephra) deposits. Applications of tephrochronology have seen significant expansion with the use of cryptotephra—low-concentration tephra deposits that are not visible in the sediment record (Lowe and Hunt 2001). The actual concentration of glass shards within cryptotephra horizons can

vary widely, from thousands to just a few per cubic centimeter in distal areas. Cryptotephra from Icelandic eruptions, for example, are being identified in increasingly distal locations throughout the North Atlantic (Abbott et al. 2011; Dugmore et al. 1995; Grönvold et al. 1995; Turney et al. 1997; Hall and Pilcher 2002; Jennings et al. 2002; Pilcher et al. 2005; Lowe 2011; Coulter et al. 2012; Balascio et al. 2011a, b; D'Andrea et al. 2012). Their wide distribution and occurrence in marine, terrestrial and glacial records represents a powerful tool for Holocene correlation in the North Atlantic.

While methodological improvements have enabled detection and isolation of very low concentrations of cryptotephra in distal areas, many of these techniques are destructive and/or labor intensive. Non-destructive approaches to searching sediment cores for tephra include magnetic susceptibility (Calanchi et al. 1998; Carter et al. 2002), X-ray radiography (Dugmore and Newton 1992), X-ray fluorescence (Kido et al. 2006; De Vleeschouwer et al. 2008; Balascio 2011), X-ray diffraction (Andrews et al. 2006), and reflectance and luminescence (Carter and Manighetti 2006). These techniques highlight textural or compositional contrasts between tephra deposits and the background sediment. Although they rapidly identify target zones, reducing the number of samples requiring further processing with extraction-microscopy procedures, these scanning methods have proven unsuitable for detecting very low concentrations of cryptotephra typical of distal deposits (Gehrels et al. 2008). Here, we investigate an alternative and novel method of non-destructively measuring cryptotephra concentrations using fluid imaging.

In this study, we test the ability of FlowCAM® technology to detect and quantify the abundance of fine volcanic glass shards in a variety of sediment samples. Our objectives are to establish the strengths and limitations of the method's ability to locate cryptotephra and measure their relative concentration and to explore its use as a potential alternative to labor-intensive, manual methods of heavy-liquids separation and microscopy.

Fluid imaging background

The Flow Cytometer and Microscope (FlowCAM®) combines the capabilities of flow cytometry, microscopy, and particle image analysis (Brown 2004;

Sieracki et al. 1998; Sterling et al. 2004; Tauxe et al. 2006). These instruments have been used primarily in biological applications to measure the size and abundance of cells (Álvarez et al. 2011 and references within; Barofsky et al. 2010; Brown 2011a, b; Buskey and Hyatt 2006; Ide et al. 2008). However, in this study we use the instrument to process sediment samples.

To process sediment samples, particles are suspended in a viscous heavy-liquid and transferred to the FlowCAM by pipette to the top of the flow cell apparatus. A peristaltic pump pulls the sample through the flow cell, where digital images of the sample are acquired at a constant rate (10 frames s^{-1}) as particles flow past a microscope lens. Images of individual grains are automatically isolated and extracted from the background image by the FlowCAM software (VisualSpreadsheet^{TM}) according to user-defined detection thresholds (Brown 2011b). Each particle image is then automatically characterized using 26 morphological properties, such as area-based spherical diameter, circularity, elongation, roughness, transparency, edge gradient, and aspect ratio (Brown 2010a). The software allows users to build a library of reference images that are most representative of the targeted particles. During sample analysis, the statistical filter assigns a score to each particle based on morphological similarity to reference examples in the library (Brown 2008). Subsequent visual inspection of these results can be performed quickly by viewing the sorted images (Brown 2010b). This semi-automated identification process reduces the time involved in standard microscopy techniques and improves reproducibility (the same libraries can be used as a reference for every sample).

In this study, we evaluate the FlowCAM's performance in distinguishing fine tephra (<63 μm diameter) from a non-volcanic sedimentary matrix. Volcanic glass particles that compose cryptotephra horizons can have a range of morphologies, but are typically distinct from other minerogenic grains (e.g. Enache and Cumming 2006). In general, the morphology of volcanic tephra shards is related to both magmatic composition and eruption style (Ersoy et al. 2007; Heiken 1972, 1974; Heiken and Wohletz 1985). They are frequently characterized by angular, vesicular shapes with concavities and troughs on grain surfaces, although the vesicles may vary in shape and density, and particle shapes can be blocky, round, or elongate. Smaller particles are often fragments of vesicle walls

and may consist of slightly curved or needle-like grains. In our application, a library of tephra images was created using samples of volcanic ash. The tephra library built for this experiment does not contain the full range of shard morphologies, but does include a wide range of angular, blocky, elongate, and vesicular grains that provides a starting point for evaluation of the method.

Methods

Instrument and software setup

Analyses in this study were performed using a Benchtop model FlowCAM at 100X magnification with a 100-μm flow cell. Before each analysis, the FlowCell was cleaned, then primed, with 15 ml of a non-fibrous and non-reactive heavy-liquid (5 % PVP, polyvinylpropyl [Sigma-Aldrich, M_w, 130,000]) to remove any air bubbles or residual particles. Camera gain and flash duration were adjusted to target an average intensity of 160–180. Samples were suspended in $\sim$20 ml of PVP and pipetted into the FlowCam with a pump setting of "4-Slow." Samples were processed using "AutoImage" mode at a constant imaging rate of 10 frames s^{-1}. At the beginning of each analysis, the first $\sim$0.25 ml of suspended sample was used to tune the instrument focus, and define the background for the automated background image subtraction. When $\sim$1 ml of sample remained in the top of the flow chamber, $\sim$10 ml of PVP were added to ensure that all particles had been imaged and the re-collection rate was $\sim$100 %. After analysis, samples were re-collected in their original containers for later use. Total time for each analysis and cleaning between samples ranged from 5 to 10 min.

Pure rhyolitic and basaltic tephra samples were processed to test the FlowCAM's ability to image cryptotephra particles <63 μm in diameter and generate a library of tephra images for use as the reference in the statistical filters (Fig. 1). Basaltic tephra samples from the Grímsvötn AD 2004 eruption (Jude-Eton et al. 2012) and rhyolitic tephra from the Askja AD 1875 eruption (Meara 2011) were used as standards. Both tephra samples were sieved to <63 μm to focus on the particle sizes typical of distal tephra deposits. Although these samples did not capture the full range

of tephra morphologies found in nature, they demonstrated the value of even a limited reference database, and provided an initial step toward building a more comprehensive database of tephra shard images that can be used for future applications.

Artificially mixed samples were also analyzed with the FlowCAM. These contained quartz-rich lake sediment (approximately 10–20 μm) and varying concentrations of tephra from the rhyolitic and basaltic sample standards. However, the abundance of fine-grained sediment decreased the FlowCAM's ability to image all particles flowing past the lens. To correct for this, we defined minimum particle size thresholds of 15 μm diameter and a 2 μm minimum distance between particles (these settings were applied to all of our analyses). This enabled the software to avoid: (i) saturating the detector with the finest particles, and (ii) imaging clusters of particles in the same frame. However, this can result in an underestimate of the final number of tephra particles identified. Applying this statistical filter, the software was able to identify basaltic and rhyolitic tephra compositions in the mixed samples. This indicated that our library could be used to identify a range of tephra compositions in sediment when particle morphologies are similar to those in the library.

Application to natural lake sediment

We performed FlowCAM analysis on a suite of lake sediment samples from a lake in Norway (69.22°N, 16.01°E) known to contain late Pleistocene finely dispersed tephra shards attributed to the Vedde Ash (rhyolitic) and Saksunarvatn tephra (basaltic) (Haflidason et al. 2000). Prior to analysis, the lake sediment samples were acidified using concentrated nitric acid to remove organic matter (Pilcher et al. 1996) and rinsed in triplicate using deionized water. Samples were then washed in deionized water over a 20-μm sieve to remove sub-20 μm particles. Heavy-liquid separations were performed to concentrate tephra shards, typically 2.3–2.5 g cm^{-3}, from the remaining mineral grains using standard methods (Turney 1998).

The concentrated lake sediment samples were processed using the FlowCAM, and re-collected into their original containers. After an initial statistical analysis using the tephra image library developed from our tephra standards, the highest-quality tephra images (i.e. in focus with well-defined edges) were
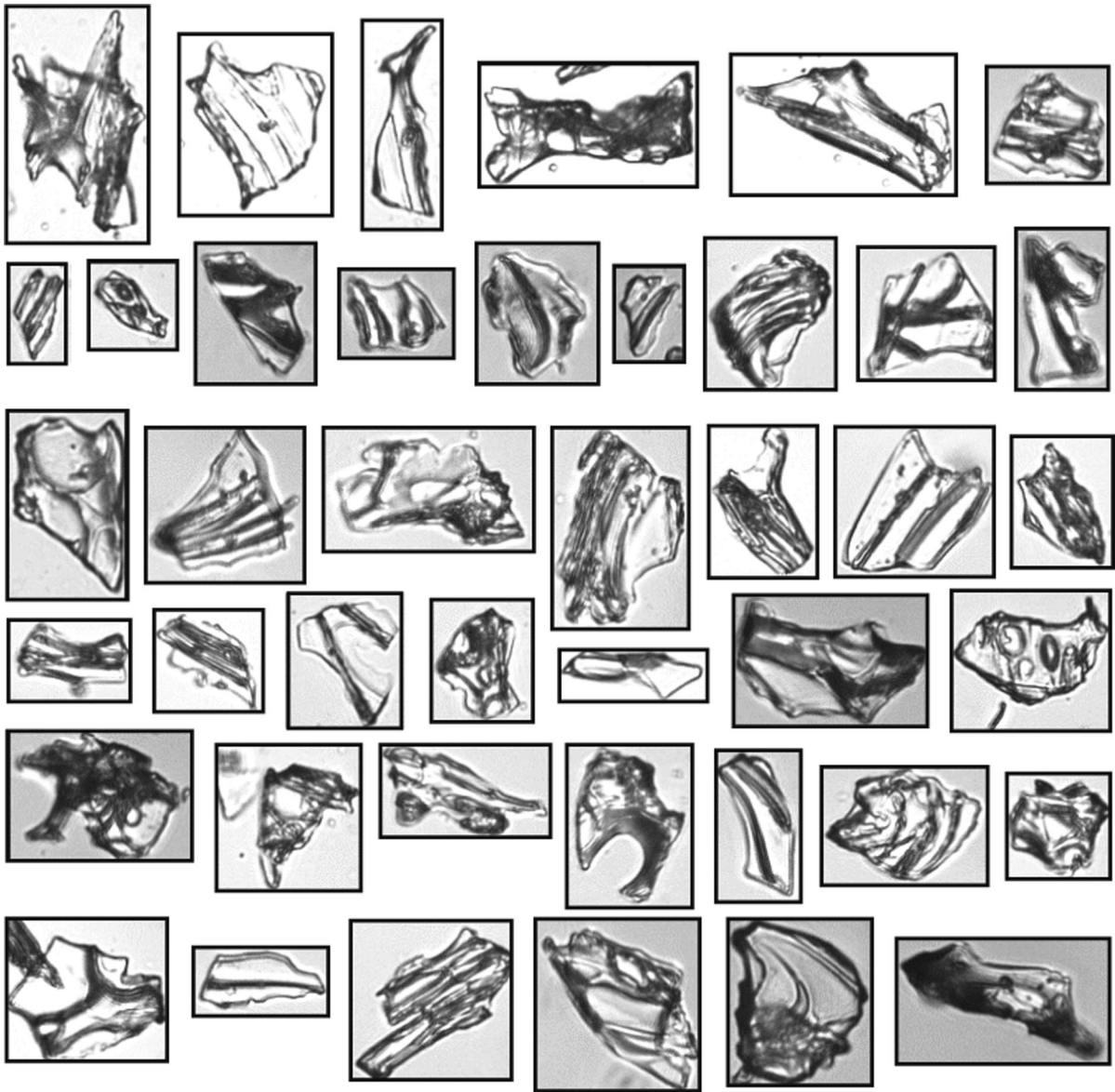
Fig. 1 Representative tephra images from the tephra image library produced by the FlowCAM

selected and added to the library. Samples were then re-analyzed using this updated image library. For each sample, images were filtered using the image library, a cutoff value was established based on inspection of the particle images, and the number of images that were determined to be tephra were summed. To determine the accuracy of this method relative to conventional methods, the re-collected samples were then mounted onto glass slides and examined under a polarized light microscope for manual counts of tephra grains.

Results

Seventeen lake sediment samples were analyzed spanning two tephra horizons previously identified by conventional methods at depth intervals of 243–250 and 283–291 cm. FlowCAM analyses show tephra concentrations ranging from 2 to 90 grains per sample, with distinct peaks of 89 and 90 grains occurring at 247 and 284 cm, respectively (Fig. 2a). Samples re-collected and examined using standard microscopy
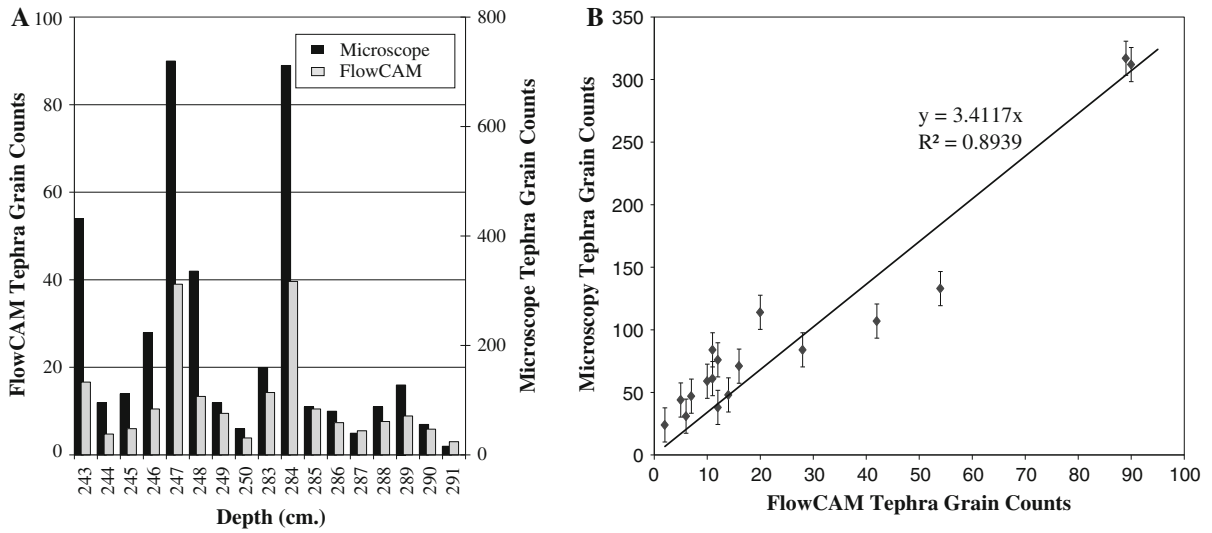
Fig. 2 **a** Grain counts for the 17 lake sediment samples using the FlowCAM (*light grey*) and traditional microscopy methods (*black*).
b Scatter plot of these values displaying a linear relationship

methods indicated concentrations ranging from 24 to 317 tephra shards per sample, with distinct peaks (317 and 312 shards) at the same depths of 247 and 284 cm that were identified by the FlowCAM analysis (Fig. 2a). Although the absolute number of grains counted on the FlowCAM was consistently lower than the microscopy counts, the relative concentrations were consistent at all depths and exhibit a linear relationship (Fig. 2b). The FlowCAM identified an average of 22.8 ± 9.7 % of the grains counted under a microscope.

To estimate the uncertainty of microscope counts, sample depths with the highest concentrations were counted under the microscope in triplicate. Average counts for the two peaks at 247 and 284 cm were 317 ± 11 and 312 ± 14, respectively. By contrast, the VisualSpreadsheet software uses an algorithm based on quantitative particle values to determine the likelihood of a particle actually being tephra, so that identification is standardized and variability in the software based identification of tephra images between multiple runs of the same sample was tested and determined to be negligible. However, the Flow-CAM images only the portion of the sediment sample that flows in the camera's limited field of view, which at 100× magnification is one-third of the sample volume (Álvarez et al. 2011). Therefore, changes in the homogeneity of the sample and very sparse quantities of tephra grains can negatively affect the reproducibility of FlowCAM based tephra counts.

Tephra counts from the FlowCAM method identified a greater percentage of shards in the samples containing basaltic tephra, 30 ± 9 %, compared with 17 ± 6 % for the rhyolitic tephra (Fig. 3a). However, for both compositions, a strong linear correlation exists between FlowCAM and traditional microscopy counts (Fig. 3b).

Discussion

The image-based, FlowCAM approach to identifying cryptotephra is capable of providing insight into relative concentrations of tephra shards. The method was effective at imaging tephra shards from 20 to 100 μm diameter, which were the limits of samples we analyzed, and at concentrations approaching zero. In lake sediment samples, comparison of FlowCAM tephra counts with standard microscopy show that the instrument was able to identify samples with the highest concentration of tephra as determined from microscope counts. However, the FlowCAM was only capable of measuring 23 ± 10 % of the microscope counts in each sample. Interestingly, in a previous study Álvarez et al. (2011) found that using the FlowCAM at 100× in autoimage mode, only 31.49 % of the total sample was being captured within the field of view of the camera lens. When taking this into account, our ability to image 23 ± 10 % of the total
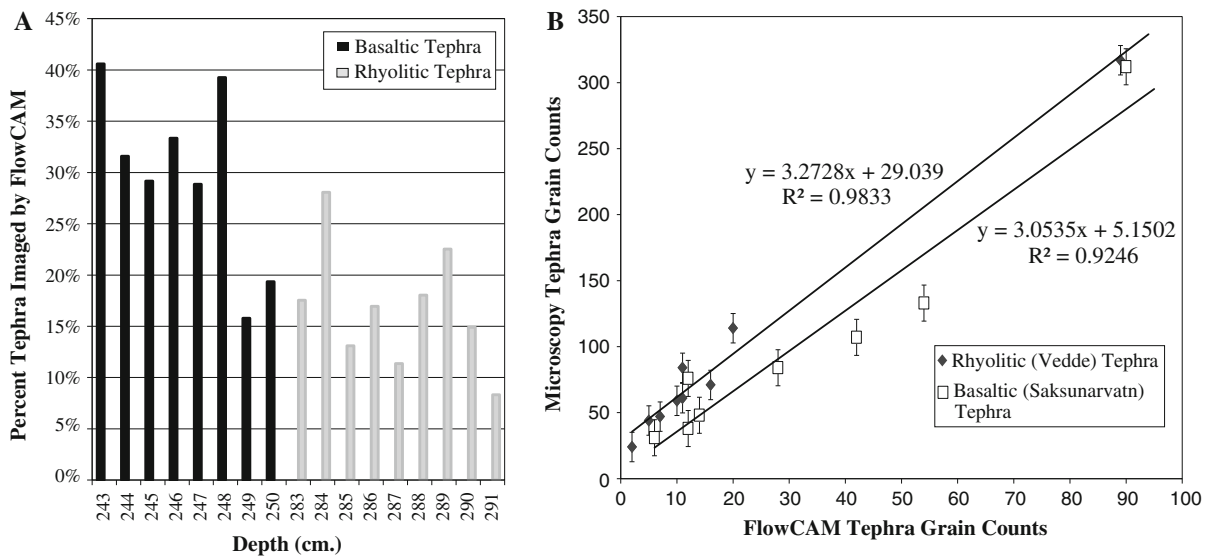
A

B

$$y = 3.2728x + 29.039$$
$$R^2 = 0.9833$$

$$y = 3.0535x + 5.1502$$
$$R^2 = 0.9246$$

Fig. 3 **a** Percent of total tephra grains imaged by the FlowCAM (FlowCAM counts/microscope counts × 100) for the rhyolitic (*light grey*) and basaltic (*black*) populations. **b** Scatter plot of

FlowCAM versus microscope counts for each population displaying linear relationships

tephra concentration not only makes sense, but also bolsters the idea that the FlowCAM is in fact imaging and correctly identifying a high percent of the tephra flowing through the field of view. When this 31.49 % field of view is corrected for in the results of this study, the FlowCAM consistently imaged and accurately identified 74.6 % of the tephra contained in each sample. Additional sources of error in the absolute number of tephra particles counted by the FlowCAM may include: the software settings used to extract particle images, particle clumping, the focus of images, and the range of tephra morphologies within the user-defined tephra image library.

The ultimate goal of this study was to test the suitability of this instrument and method as a replacement for the laborious and destructive extraction-microscopy technique. This was under the assumption that an unprocessed sample of lake sediment could be rapidly analyzed by the FlowCAM, and subsequently re-collected, preserving the sample for later analyses. However, our study showed that ratios of tephra to background sediment had to exceed $\sim$1:200 to be processed in a reasonable amount of time (20–30 min per sample). In contrast, distal cryptotephra deposits occur in very low concentrations and may not be suitable for FlowCAM analysis. In sedimentary archives where cryptotephra horizons contain very

high concentrations of tephra shards this method would be advantageous. However, analysis of small sediment volumes ($\sim$1 cm^3) with low tephra concentrations limit the number of particles counted in a reasonable amount of time. Thus, pre-processing of the sediment core is still required to reduce the sample to a manageable volume prior to FlowCAM analysis. Nevertheless, the FlowCAM can provide an indication of where tephra is likely to be more abundant in a sediment core—making subsequent isolation of tephra shards using conventional density-separation methods more efficient by focusing attention on specific depth horizons. In other types of records (peat, or sedimentary records with visible/high concentrations of tephra), the FlowCAM's possibility as an effective replacement to standard microscopy seems very possible, and warrants further investigation in future studies.

Limitations and recommendations

Our study demonstrates that the FlowCAM is able to detect tephra shards and may be useful in cryptotephra applications. However, the ability to distinguish tephra in sediment is dependent on the quality of the user-defined library of tephra images and the difference in the morphology of tephra from the background

sediment. In applying this method, we recommend that care be taken to build a library of tephra images that captures a range of tephra morphologies predicted for a particular environment or region. If the library is inadequate, this method may fail to detect tephra even if it is present. For example, diagenetically altered, crystal-rich, lithic-rich or phreatomagmatic tephras containing fewer of the distinctive bubble wall shard morphologies may be challenging to account for, but present an interesting area for future work in fine-tuning the FlowCAM technique. Additionally, uncertainties in particle counts may be reduced with additional preparation steps to disaggregate samples, such as the use of a dispersant (Calgon) and/or sonication prior to FlowCAM analysis.

Conclusions

The results from this study indicate a strong potential for the FlowCAM to provide a valuable method of particle discrimination in a wide variety of sedimentological applications. Further investigation of the utility and reproducibility of the results is necessary. However, the instrument was able to efficiently capture high-quality images of tephra shards within a sample, and that the images clearly depicted the distinct morphological characteristics of the targeted tephra shards. These distinct particle properties allowed the visual pattern recognition software to identify and separate the tephra images within a sample's data file. We were able to accurately determine the relative concentrations of tephra within a sediment sample, although the absolute tephra concentrations were consistently underestimated. The primary reason for lower tephra counts using the FlowCAM is because of the camera's limited field of view, which has been established by others and can be used to correct particle counts. Further investigation of the applications and limitations of the instrument in cryptotephra studies could address: (i) a greater number of tephra standards, (ii) additional background sediment types, and (iii) particle grain sizes. The FlowCAM may also provide an alternative approach to traditional microscopy methods when the identification and enumeration of any microscopic "group" of particles in a mixed sediment sample can be defined by a set of distinct set of particle characteristics.

References

Abbott PM, Davies SM, Austin WEN, Pearce NJG, Hibbert FD (2011) Identification of cryptotephra horizons in a North East Atlantic marine record spanning marine isotope stages 4 and 5a (60,000–82,000 a b2k). Quat Int 246:177–189

Álvarez E, Lopez-Urrutia Á, Nogueira E, Fraga S (2011) How to effectively sample the plankton size spectrum? A case study using the FlowCAM. J Plankton Res 33:1119–1133

Andrews JT, Eberl DD, Kristjansdottir GB (2006) An exploratory method to detect tephras from quantitative XRD scans: examples from Iceland and east Greenland marine sediments. Holocene 16:1035–1042

Balascio NL (2011) Lacustrine records of Holocene climate and environmental change from the Lofoten Islands, Norway. Ph.D. Dissertation. University of Massachusetts Amherst

Balascio NL, Wickler S, Narmo LE, Bradley RS (2011a) Distal cryptotephra found in a Viking boathouse: the potential for tephrochronology in reconstructing the Iron Age in Norway. J Archaeological Sci 38:934–941

Balascio NL, Zhang Z, Bradley RS, Perren B, Dahl SO, Bakke J (2011b) A multi-proxy approach to assessing isolation basin stratigraphy from the Lofoten Islands, Norway. Quat Res 75:288–300

Barofsky A, Simonelli P, Vidoudez C (2010) Growth phase of the diatom Skeletonema marinoi influences the metabolic profile of the cells and the selective feeding of the copepod Calanus spp. J Plankton Res 32:263–272

Brown L (2004) Continuous imaging fluid particle analysis—a primer. Fluid imaging technologies white paper. http://fluidimaging.com

Brown L (2008) Particle image understanding—a primer. Fluid Imaging Technologies, Yarmouth, ME

Brown L (2010a) VisualSpreadsheet©: intelligent pattern recognition for particle analysis. Fluid Imaging Technologies VisualSpreadsheet© Particle Analysis Software Product Literature. http://fluidimaging.com

Brown L (2010b) VisualSpreadsheet©: interactive, intuitive particle analysis software. Fluid Imaging Technologies VisualSpreadsheet© Particle Analysis Software Product Literature. http://fluidimaging.com

Brown L (2011a) Characterizing biologics using dynamic imaging particle analysis. BioPharm Int 24:4–9

Brown L (2011b) FlowCAM tech brief: proper thresholding of transparent particles. Fluid imaging technologies tech briefs. http://fluidimaging.com

Buskey EJ, Hyatt CJ (2006) Use of the FlowCAM for semiautomated recognition and enumeration of red tide cells (Karenia brevis) in natural plankton samples. Harmful Algae 5:685–692

Calanchi N, Cattaneo A, Dinelli E, Gasparotto G, Lucchini F (1998) Tephra layers in late quaternary sediments of the central Adriatic Sea. Mar Geol 149:191–209

Carter L, Manighetti B (2006) Glacial/interglacial control of terrigenous and biogenic fluxes in the deep ocean off a high input, collisional margin: a 139 kyr-record from New Zealand. Mar Geol 226:307–322

Carter L, Manighetti B, Elliot M, Trustrum N, Gomez B (2002) Source, sea level and circulation effects on the sediment flux to the deep ocean over the past 15 ka off eastern New Zealand. Glob Planet Change 33:339–355

D'Andrea WJ, Vaillencourt DA, Balascio NL, Werner A, Roof SR, Retelle M, Bradley RS (2012) Mild little ice age and unprecedented recent warmth in an 1800 year lake sediment record from Svalbard. Geology 40:1007–1010

De Vleeschouwer F, van Vliët-Lanoé B, Fagel N, Richter T, Boës X (2008) Development and application of high-resolution petrography on resin-impregnated Holocene peat columns to detect and analyse tephras, cryptotephras, and other materials. Quat Int 178:54–67

Dugmore AJ, Newton AJ (1992) Thin tephra layers in peat revealed by X-radiography. J Archaeol Sci 19:163–170

Dugmore AJ, Larsen G, Newton AJ (1995) Seven tephra isochrones in Scotland. The Holocene 5:257–266

Enache MD, Cumming BF (2006) The morphological and optical properties of volcanic glass: a tool to assess density-induced vertical migration of tephra in sediment cores. J Paleolimnol 35:661–667

Ersoy O, Gourgaud A, Aydar E, Chinga G, Thouret J-C (2007) Quantitative scanning-electron microscope analysis of volcanic ash surfaces: application to the 1982–1983 Galunggung eruption (Indonesia). Geol Soc Am Bull 119:743–752

Gehrels MJ, Newnham RM, Lowe DJ, Wynne S, Hazell ZJ, Caseldine C (2008) Towards rapid assay of cryptotephra in peat cores: review and evaluation of various methods. Quat Int 178:68–84

Grönvold K, Óskarsson N, Johnsen SJ, Clausen HB, Hammer CU, Bond G, Bard E (1995) Ash layers from Iceland in the Greenland GRIP ice core correlated with oceanic and land sediments. Earth Planet Sci Lett 135:149–155

Haflidason H, Eiriksson J, Van Kreveld S (2000) The tephrochronology of Iceland and the North Atlantic region during the Middle and Late Quaternary: a review. J Quat Sci 15:3–22

Hall VA, Pilcher JR (2002) Late-Quaternary Icelandic tephras in Ireland and Great Britain: detection, characterization and usefulness. Holocene 12:223–230

Heiken G (1972) Morphology and petrography of volcanic ashes. Geol Soc Am Bull 83:1961–1988

Heiken G (1974) An atlas of volcanic ash. Smithson Contrib Earth Sci 12:1–101

Heiken G, Wohletz KH (1985) Volcanic ash. University of California Press, Berkeley, CA

Ide K, Takahashi K, Kuwata A, Nakamachi M, Saito H (2008) A rapid analysis of copepod feeding using FlowCAM. J Plankton Res 30:275–281

Jennings AE, Gronvold K, Hilberman R, Smith M, Hald M (2002) High resolution study of Icelandic tephras in the Kangerlussuaq trough, southeast Greenland, during the last deglaciation. J Quat Sci 17:747–757

Jude-Eton T, Thordarson T, Gudmundsson MT, Oddsson B (2012) Dynamics, stratigraphy and proximal dispersal of supraglacial tephra during the ice-confined 2004 eruption at Grímsvötn Volcano, Iceland. Bull Volc 74:1057–1082

Kido Y, Koshikawa T, Tada R (2006) Rapid and quantitative major element analayis method for wet fine-grained sediments using and XRF microscanner. Mar Geol 229:209–225

Lowe DJ (2011) Tephrochronology and its application: a review. Quat Geochron 6:107–153

Lowe DJ, Hunt JB (2001) A summary of terminology used in tephra-related studies. Les Dossiers de l'Archeo-Logis 1:17–22

Meara R (2011) Climatic and environmental impact of Holocene silicic explosive eruptions in Iceland. Ph.D. Thesis. University of Edinburgh, p 324

Pilcher JR, Hall VA, McCormac FG (1996) An outline tephrochronology for the Holocene of the north of Ireland. J Quat Sci 11:485–494

Pilcher J, Bradley RS, Francus P, Anderson L (2005) A Holocene tephra record from the Lofoten Islands, Arctic Norway. Boreas 34:136–156

Sieracki C, Sieracki ME, Yentsch CS (1998) An imaging-in-flow system for automated analysis of marine microplankton. Mar Ecol Prog Ser 168:285–296

Sterling MC Jr, Bonner JS, Ernest ANS, Page CA, Autenrieth RL (2004) Characterizing aquatic sediment–oil aggregates using in situ instruments. Mar Poll Bull 48:533–542

Tauxe L, Steindorf JL, Harris A (2006) Depositional remanent magnetization: toward an improved theoretical and experimental foundation. Earth Planet Sci Lett 244:515–529

Turney CSM (1998) Extraction of rhyolitic component of Vedde microtephra from minerogenic lake sediments. J Paleolimnol 19:199–206

Turney CSM, Harkness DD, Lowe JJ (1997) The use of microtephra horizons to correlate Late-glacial lake sediment successions in Scotland. J Quat Sci 12:525–531